Icarus 263 (2016) 2–9

Contents lists available at ScienceDirect

Icarus

journal homepage: www.journals.elsevier.com/icarus

# Saturn kilometric radiation intensities during the Saturn auroral campaign of 2013

W.S. Kurth [a,*], G.B. Hospodarsky [a], D.A. Gurnett [a], L. Lamy [b], M.K. Dougherty [c], J. Nichols [d], E.J. Bunce [d], W. Pryor [e], K. Baines [f], T. Stallard [d], H. Melin [d,g], F.J. Crary [h]

[a] University of Iowa, Dept. of Physics and Astronomy, Iowa City, IA 52242, USA
[b] LESIA, Observatoire de Paris, CNRS, UPMC, Universit Paris Diderot, Meudon, France
[c] Imperial College of Science, Technology and Medicine, Space and Atmospheric Physics Group, Department of Physics, London SW7 2BW, UK
[d] University of Leicester, Department of Physics and Astronomy, Leicester LE1 7RH, UK
[e] Central Arizona College, Department of Science, Coolidge, AZ 85128, USA
[f] Jet Propulsion Laboratory, 4800 Oak Grove Drive, Pasadena, CA 91109, USA
[g] Space Environment Technologies, Planetary and Space Science Division, 320 N. Halstead Street, Suite 110, Pasadena, CA 91107, USA
[h] Laboratory for Atmospheric and Space Physics, University of Colorado Boulder, 1234 Innovation Drive, Boulder, CO 80303, USA

ARTICLE INFO

*Article history:*
Received 29 August 2014
Revised 11 December 2014
Accepted 8 January 2015
Available online 20 January 2015

*2014 MSC:*
00-001
00-00

*Keywords:*
Saturn, magnetosphere
Aurorae
Solar wind
Radio observations

ABSTRACT

The Saturn auroral campaign carried out in the spring of 2013 used multiple Earth-based observations, remote-sensing observations from Cassini, and in situ-observations from Cassini to further our understanding of auroras at Saturn. Most of the remote sensing and Earth-based measurements are, by nature, not continuous. And, even the in situ measurements, while continuously obtained, are not always obtained in regions relevant to the study of the aurora. Saturn kilometric radiation, however, is remotely monitored nearly continuously by the Radio and Plasma Wave Science instrument on Cassini. This radio emission, produced by the cyclotron maser instability, is tightly tied to auroral processes at Saturn as are auroral radio emissions at other planets, most notably Jupiter and Earth. This paper provides the time history of the intensity of the radio emissions through the auroral campaign as a means of understanding the temporal relationships between the sometimes widely spaced observations of the auroral activity. While beaming characteristics of the radio emissions are known to prevent single spacecraft observations of this emission from being a perfect auroral activity indicator, we demonstrate a good correlation between the radio emission intensity and the level of UV auroral activity, when both measurements are available.


## 1. Introduction

One of the challenges of carrying out auroral campaigns at the outer planets is that of knowing the solar wind input to the magnetosphere. At Earth there are often one or more solar wind monitors available to provide input for magnetospheric studies, whether for studies of the aurora, the dynamics of the radiation belts, or other aspects of the Sun-magnetosphere interaction.

Given the relationship between auroral kilometric radiation and terrestrial aurora which has been studied at length since the early 1970s (Gurnett, 1974; Voots et al., 1977; Huff et al., 1988; Murata et al., 1997; Kurth and Gurnett, 1998; Kurth et al., 1998), it was recognized that the intensity of such auroral radio emissions provided a more-or-less continuous monitor of the level of auroral activity and can serve as a proxy for such indices as the auroral electrojet AE.

Without a solar wind monitor, it is difficult to extend the experiences at Earth to the outer planets and assess the role of the solar wind in outer planet magnetospheric dynamics. For example, there are variations in the intensity of the various radio components at Jupiter, some of the most intriguing and interconnected are those studied by Louarn et al. (2000, 2001, 2014) in which it appears that certain energetic events are reflected in intensifications of the auroral hectometric radio emissions, the onset of narrowband emissions from the outer edge of the Io torus, and the thinning of the distant plasma sheet as reflected in vertical density profiles of the plasmasheet revealed by trapped continuum radiation. While the common interpretation of these quasi-periodic energetic events is that they represent the shedding of Iogenic mass which loads the magnetosphere and likely represents a largely

* Corresponding author.
*E-mail address:* william-kurth@uiowa.edu (W.S. Kurth).

http://dx.doi.org/10.1016/j.icarus.2015.01.003
0019-1035/

internally-driven set of dynamics, the lack of good solar wind monitoring during the Galileo mission meant that there was no way to identify the possibility of solar influence on the process.

It is notable that during a short period in 2000–2001 Cassini provided the solar wind dynamics measurements required for addressing the importance of this input to jovian magnetospheric dynamics. Gurnett et al. (2002) showed that interplanetary shocks were effective in the intensification of jovian radio emissions. And, Hess et al. (2014) have completed a fairly exhaustive analysis of the response of jovian radio emissions observed by Cassini, Galileo, and the Nançay decameter array in conjunction with in situ Cassini magnetic field measurements as Cassini approached Jupiter in late 2000. This study showed a good correspondence between the arrival of interplanetary shocks and the initiation of radio emissions.

Saturn is nearly 10 AU from the Sun and the prospects of using solar wind models to project observations at 1 AU to Saturn are rather bleak unless Saturn is within ~60 degrees of the 1 AU monitor (usually spacecraft upstream of Earth) although an alignment within 30 degrees is better (Zieger and Hansen, 2008). At Saturn, the two Voyagers were used together to understand Saturn's magnetospheric interaction with the solar wind. The non-encountering spacecraft was close enough to serve as a solar wind monitor for the encountering spacecraft. The Voyager 1/Voyager 2 tag-team approach was rather successful in understanding, for example, the importance of the solar wind input (speed, density, dynamic pressure) on the intensity of Saturn kilometric radiation (SKR) which is Saturn's auroral radio component (Desch, 1982). In fact, this approach yielded the best evidence available that Saturn was immersed in Jupiter's magnetotail during the Voyager 2 encounter (Desch, 1983).

In a notable campaign investigators took advantage of Cassini's 6-month long approach to Saturn in the first half of 2004 to monitor the solar wind at Saturn's distance, while an intensive campaign of monitoring Saturn's auroras was carried out by the Hubble Space Telescope (HST) and while the Cassini Radio and Plasma Wave Science (RPWS) instrument (Gurnett et al., 2004) monitored SKR intensities. This campaign provided anecdotal evidence of the enhancement of SKR during times of intensified auroras in response to enhancements in the solar wind pressure, often in the form of poleward expansion of the usually narrow dawn side aurora (Kurth et al., 2005; Crary et al., 2005; Clarke et al., 2005). The integrated power in SKR $P_{SKR}$ over 10 kHz to 1 MHz was compared to the estimated power input to the UV aurora $P_{UV}$. While a positive correlation was found, most of the UV observations were obtained when emissions were weak and the basis of the correlation relied heavily on only two measurements at significantly higher intensities. Another study benefitting from this approach series of observations characterized the usual response of SKR emissions to solar wind compressions as low-frequency extension (LFE) events (Badman et al., 2008). In these events, not only did the intensity of the radio emissions increase near the time of magnetospheric compression events, but the spectrum of the SKR broadened, most notably to lower frequencies, hence the term low-frequency extension. Jackman et al. (2009) interpret such LFEs as the expansion of the auroral acceleration region to higher altitudes (hence lower SKR frequencies) due to an increase in current densities between the ionosphere and magnetosphere driven by substorm-like events. Bunce et al. (2005b) examined the reaction of the magnetosphere to a magnetospheric compression, as identified with an SKR LFE. Other studies of the response of the UV aurora and SKR to the solar wind include Clarke et al. (2009) and Lamy et al. (2009). The latter paper provides the statistical UV/radio spatial conjugacy which justifies the calculation of correlation coefficients.

Lamy et al. (2013) took advantage of intensive auroral observations by Cassini in January 2009 at radio, ultraviolet and infrared wavelengths to study the aurora over a planetary rotation. This exhaustive study, among other things, assessed the energy budget of the aurora on Saturn and examined the details of how radio beaming affects the detected SKR intensity relative to the observed UV radiation. This paper addresses the ways in which SKR beaming complicates the interpretation of an instantaneous radio measurement of auroral activity. In fact, they estimate via simulations that only a few percent of the SKR sources are visible at any instant in time and that, similarly, only a few percent of the SKR power is visible, instantaneously. Lamy et al. establish the relation of SKR sources to auroral spots and model the observed spectrum as those spots rotate under the observer, taking into account the beaming properties of the SKR cyclotron maser instability mechanism. They conclude that a rotational average is justified since it averages the visibility of each of the radio sources as they rotate. They also compute a rank correlation coefficient between the SKR and UV power radiated that ranged from 0.74 to 0.78 with better correlations being achieved when averaging over the time needed for corotating radio sources to rotate so that the entire spectrum of sources on a single field line are observed.

It is important to note that Saturn kilometric radiation exhibits modulation periods in the range of 10.6–10.8 h that are likely related to, but not directly indicative of the planetary rotation rate. Desch and Kaiser (1981) originally reported a period of 10.66 h in the SKR and this was taken to be Saturn's rotation period. However, Lecacheux et al. (1997) showed that the SKR period varied by of order 1% on time scales of months and years, hence, could not be the actual rotation period. Kurth et al. (2008) showed that there were two modulation periods of the SKR and Gurnett et al. (2009) showed that a period of about 10.8 h was associated with radio emissions in the southern hemisphere and one of about 10.6 h was associated with northern SKR. Lamy (2011) provides a concise overview of the variability of the northern and southern periodicities. The intensifications studied in this paper generally stand out from these diurnal variations, although the multiplicity of periods adds to the complexity.

## 2. Saturn kilometric radiation observations during the spring 2013 campaign

The spring 2013 Saturn auroral campaign took place from early April through late May 2013 and included in situ and remote observations from Cassini instruments (Magnetometer (MAG)) (Dougherty et al., 2004); Magnetospheric Imaging Instrument (MIMI) (Krimigis et al., 2004); Radio and Plasma Wave Science (RPWS) (Gurnett et al., 2004), Visual and Infrared Mapping Spectrometer (VIMS) (Brown et al., 2004); Ultraviolet Imaging Spectrograph (UVIS) (Esposito et al., 2004); and Imaging Science Subsystem (ISS) (Porco et al., 2004). HST Advanced Camera for Surveys (ACS) observations, ground-based observations including Keck and IRTF, solar wind modeling were all involved, as well.

Fig. 1 shows Cassini RPWS observations of radio emissions above 4 kHz for an interval from 2 April to 22 May (days 092–142) 2013, an interval covering the Saturn auroral campaign of 2013. The power flux of radio emissions scaled to a distance of 1 astronomical unit (AU) is shown according to the color bar on the right as a function of frequency and time. Superposed on the spectrogram is a white trace which is a 10-h sliding average integrated power from 20 kHz to 1 MHz slid by 1 h increments. Each of the two panels have a duration of 25 days, approximately the solar rotation period as viewed at Saturn. By doing so, we have identified a recurring pattern of intensifications of SKR reflecting what we believe to be a pattern of compressions associated with corotating interaction regions (CIRs) in a basic two-sector solar wind. Source surface synoptic charts from the Wilcox Solar Observatory for Carrington Rotation 2135 (starting on March 21, 2013) and

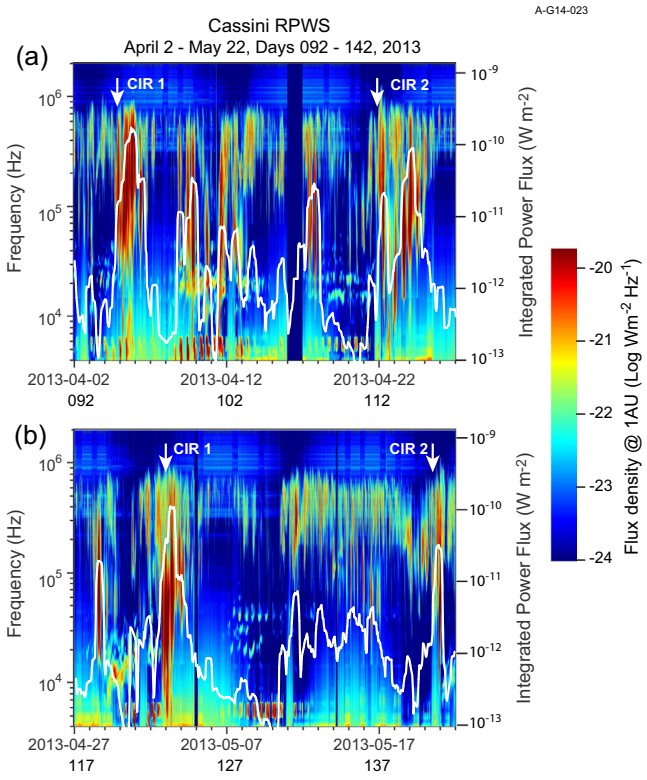


**Fig. 1.** Saturn kilometric radiation observations over the spring 2013 Saturn auroral campaign. The intensity of the radio emissions as a function of frequency in time is coded according to the color bar on the right. The superposed white trace is a sliding 10-h integration of SKR power from 20 kHz to 1 MHz scaled to a distance of 20 $R_S$. Panel (a) shows observations from a 25-day interval beginning with April 2, 2013. Panel (b) includes the 25-day interval beginning with April 27. Apparently repeating intervals of enhanced SKR activity are identified as due to the likely passage of CIRs associated with a two-sector solar wind. The two sets of arrows labeled CIR 1 and CIR 2 are separated by about 28 days and represent the approximate onset times of the intensifications on days 094 and 122 for CIR 1 and days 112 and 140 for CIR 2. The departure from the expected 25-day period is discussed in Section 2.

neighboring rotations show a stable two-sector structure at the Sun. The recurrence period of the identified features in Fig. 1 is closer to 28 days than the expected 25. We note that similar variations from the expected period are reported by Jackman et al. (2005) in their Fig. 3. Burlaga et al. (2003) discuss the Corotating Merged Interaction Region (CMIR) zone between 5 and 25 AU and give model results and also Voyager observations near 15 AU that show a broad peak in the B/⟨B⟩ spectrum at 26 days, where ⟨B⟩ is the yearly average magnitude of **B**. A period of 28 days is well within this broad peak.

The high pressure streams at the sector interfaces compress the magnetosphere and cause intensifications of the SKR (Jackman et al., 2005) often resulting in SKR LFEs (Badman et al., 2008). This structure is also discussed by Hsu et al. (2016). There are additional intensifications of SKR in Fig. 1 that may be associated with other compressional structures in the solar wind not related to the CIRs or due to internal dynamics in Saturn's magnetosphere (Jackman et al., 2009), an example of which was identified by Lamy et al. (2013) on day 028 of 2009. We present the campaign here in three sub-intervals and concentrate on the SKR measurements and related HST images.

### 2.1. April 4–7, 2013

The initial interval included in the spring 2013 Saturn auroral campaign includes only one visit on 5 April (day 095) 2013 for HST imaging, hence, does not provide, on its own, the possibility for studying the dynamics of Saturn's aurora. However, it does provide observations during the passage of a corotating interaction region (see Fig. 1). Fig. 2 shows Cassini RPWS observations of SKR for the interval 4–7 April (days 094–097) 2013. The frequency range of the spectrogram is 4 kHz to 2 MHz, designed to include the full range of SKR emissions, including the LFEs that are indicative of magnetospheric compressions. It should be noted that while the primary emissions appearing in this spectrogram are SKR, there are sometimes a series of narrowband emissions centered near 5 kHz and also in the range of 20–30 kHz that appear. These emissions are not spectrally related to the SKR, however, Louarn et al. (2007) suggest that they may be temporally related via magnetospheric dynamics in a sense similar to the relation of nKOM to HOM intensifications at Jupiter (Louarn et al., 2000, 2001, 2014). The narrowband emissions have been studied extensively by Ye et al. (2009, 2010) and Wang et al. (2010).

Superposed on the spectrogram is a white trace that represents the integrated SKR power flux as a function of time. Because of the expanded time scale compared to Fig. 1, the integrated power flux is computed by integrating from 20 kHz to 1 MHz using a sliding 1-h average every 10 min. No attempt is made to filter the narrowband emissions, but the relatively low amplitude and small bandwidth limits the effect of them on the integrated power. Note that the smaller averaging interval results in somewhat larger peaks than those shown in Fig. 1. Because the detected power will fall with the distance to the source, $r$, as $r^{-2}$, the integrated power is scaled to 20 $R_S$. However, this correction assumes the source is at the center of Saturn, hence, when Cassini is very close to Saturn, this correction is suspect depending on the actual source position and its distance from the spacecraft. It should be noted that Cassini executed a close flyby (altitude 1400 km) of Titan at 21:44 on 5 April. As is often the case, Titan's high density ionosphere can occult some or all of the SKR sources, hence, a decrease in the SKR amplitude near Titan closest approach is due to such an occultation. The peak integrated power flux (1-h average) approaches $10^{-9}$ W m$^{-2}$ late on 5 April (day 095), but is high over most of the day. In fact, the power fluxes in this interval exceed the 1% occurrence level reported by Lamy et al. (2008). The SKR

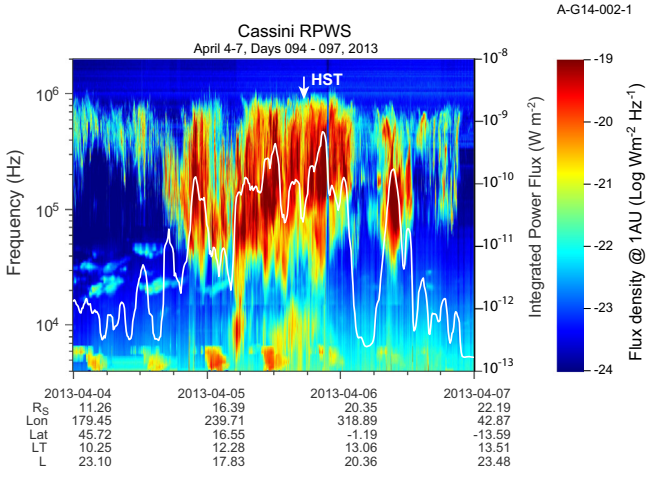


**Fig. 2.** SKR observations for the day 094–097 interval showing extensive auroral activity beginning late on day 094 and continuing for most of the interval. The white trace shows 1-h sliding averages of SKR power integrated from 20 kHz to 1 MHz. This auroral activity is thought to be initiated by the interaction of a corotating interaction region (CIR 1 as indicated in Fig. 1) compressing the magnetosphere. An auroral image captured by HST at the time of the arrow is given in Fig. 3.

bandwidth expands to lower frequencies at ~05:00 UT well before the time of the Titan flyby.

One can ask exactly where in the interval covered by Fig. 2 the solar wind compression interacts with the magnetosphere. In this paper we have identified times labeled CIR *n* as the onset of an interval of enhanced SKR activity. With no close-by solar wind monitor, we cannot unambiguously answer this question. We can, however, return to the early study by Desch (1982) in which a good correlation between the solar wind pressure and SKR intensity is shown to suggest that the solar wind compression may be an extended event and not necessarily instantaneous.

As shown in Fig. 3, HST acquired an image of Saturn's north pole centered on 17:35:32 (with the one-way light travel time from Saturn subtracted from the time recorded at HST), close to the time when the SKR power is at its greatest. In this image, the dawnside UV aurora is clearly intensified and has expanded poleward from its usually narrow form to about 85° latitude, very similar to the response of the aurora to solar wind compression events observed by Prangé et al. (2004) in late 2000 and in 2004 during the Cassini approach campaign (Clarke et al., 2005). Nichols et al. (2009) find the mean equatorward edge of the northern auroral oval to occur at a co-latitude of 16.3°, or at 73.7° latitude, not dissimilar to that in Fig. 3. The nominal auroral oval, however is only 1–2° wide (Badman et al., 2016). Note that the HST images included here are as viewed from Earth, or approximately from the perspective of the Sun. 2013 is some 4 years past equinox, so the north pole is tilted toward the Sun (or Earth).

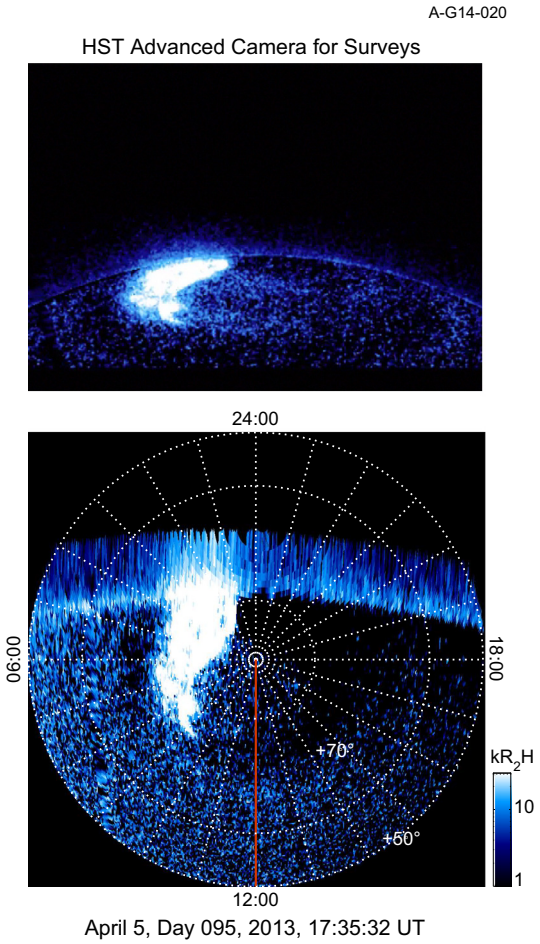


**Fig. 3.** A UV image from the HST Advance Camera for Surveys showing the poleward expansion and brightening of Saturn's aurora obtained at the time indicated by the arrow in Fig. 2. The upper panel is the image acquired by HST from its position near Earth. The lower panel is a projection onto Saturn's north pole with latitudes and local times noted.

### 2.2. April 18–24, 2013

The second interval we discuss has significantly more intensive and extensive auroral imaging from HST utilizing 6 HST orbits. Fig. 4 gives a summary of the SKR observations similar to Fig. 2 in the range April 18–24 (days 108–114), again with the integrated SKR power averaged over 1-h intervals. The early portion of the interval is relatively quiet in the SKR frequency range, but activity increases in the last two days, or so, of the interval. Again, the peak integrated 1-h average power flux approaches $10^{-9}$ W m$^{-2}$ near 07:20 UT on 22 April (day 112). These emissions are right-hand polarized (not shown here) indicating extraordinary mode emission from the northern hemisphere. This peak is, again, attributed to a compression associated with a CIR as indicated in Fig. 1. Notice that the time since the proposed CIR compression in Fig. 2 is about 17 days, not an unreasonable time separation for the CIR assumption and a two-sector structure to the solar wind (c.f. Jackman et al., 2005).

Fig. 5 shows two of the HST images of the northern hemisphere obtained during this portion of the campaign at times marked in Fig. 4. Fig. 5a is from 21 April (day 111) at 13:47:42 UT and prior to the compression event. The auroral oval is quite thin with some dawnside brightening and a smaller region of brightening in the post-dusk sector. Fig. 5b was acquired on 22 April (day 112) at 08:35:54 UT, very close to the peak in the SKR integrated power shown in Fig. 4 and after the magnetosphere has been compressed. At this time the dawnside oval is brighter and there is a clear deviation from a simple, narrow oval just pre-noon. A much more complete discussion of the HST observations is provided by Nichols et al. (2014) and in situ observations obtained during this event are discussed in detail by Badman et al. (2016).

### 2.3. May 16–23, 2013

The third interval in the campaign runs from 16–23 May (days 136–143) 2013 and includes 8 HST orbits. Fig. 6 summarizes the SKR observations for the interval in the same format as Figs. 2 and 4. The strongest SKR in this interval occurs near the end of May 20 (day 140) near 18:40 UT and again approaches $10^{-9}$ W m$^{-2}$ and exceeds the 1% occurrence level reported by

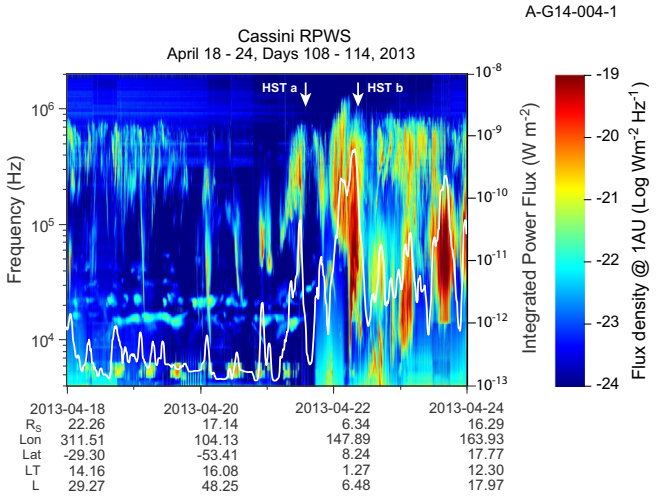


**Fig. 4.** SKR observations similar in format to Fig. 2. HST images for the times noted by the arrows are given in Fig. 5.

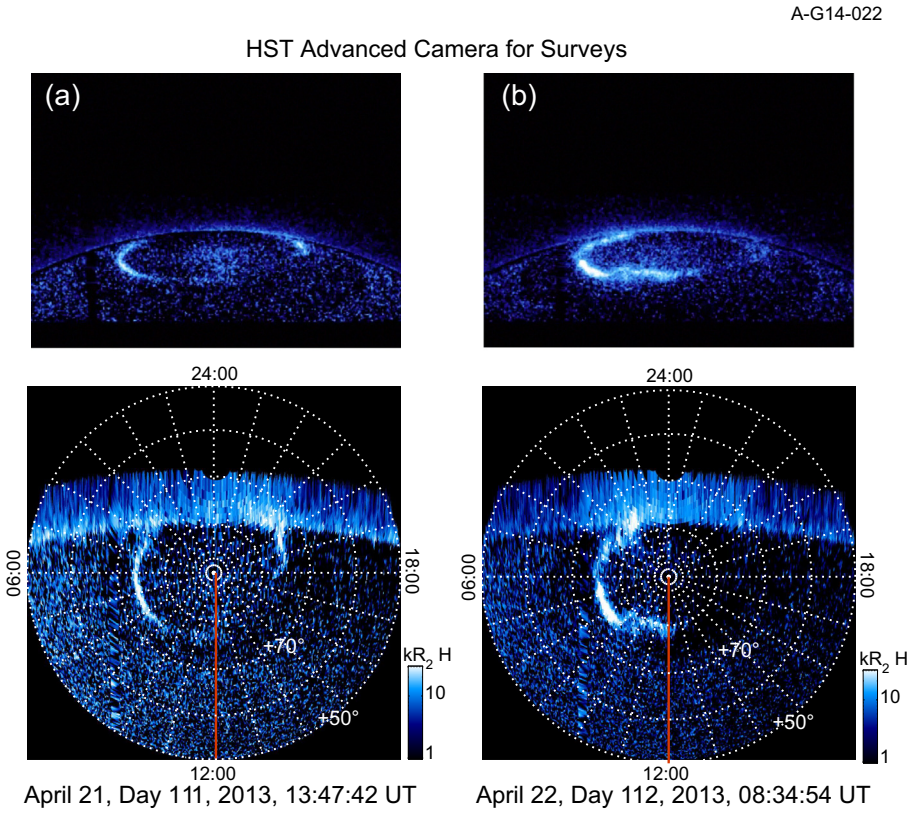


**Fig. 5.** HST images taken at two times as indicated in Fig. 4 showing the evolution of the morphology and brightness of Saturn's aurora. We suspect the earlier image was acquired prior to the compression event and the latter, somewhat after.

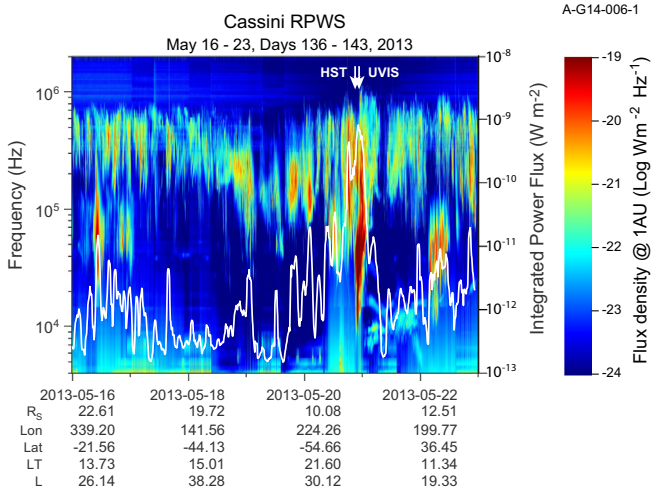


**Fig. 6.** Observations of SKR and integrated intensity for the interval covering days 136 to 143, 2013. Indicated by arrows at the top are when images were captured by HST (see Fig. 7) and UVIS (see Fig. 8). This peak in SKR power flux is associated with the second appearance of CIR 2 as shown in Fig. 1.

Lamy et al. (2008). The polarization is, again, right-hand, indicating a northern hemisphere source. Note, however, that using the 10-h averages used in Fig. 1, the peak power flux for this event is a bit lower than the previous two events at about $4 \times 10^{-10}$ W m$^{-2}$. This intensification is also believed to be related to a CIR, coming about 28 days after the CIR-related event in Fig. 4. In addition, there are brief intensifications on 16 May (day 136) and 22 May (day 142) at much lower peak power fluxes of approximately $1.5 \times 10^{-11}$ W m$^{-2}$ and $9 \times 10^{-12}$ W m$^{-2}$, respectively.

The HST image shown in Fig. 7 obtained just prior to the peak SKR power on 20 May (day 140) was taken at 20:51:01 UT and shows brightening slightly poleward of the also-visible dawnside oval as well as a poleward feature in the late morning which might be argued to be associated with the cusp (c.f. Bunce et al., 2005a; Clarke et al., 2005; Gérard et al., 2005; Grodent et al., 2005). Cassini's UVIS obtained an image about two hours later at 22:54 UT shown in Fig. 8. Of course, the perspective of Cassini is radically different than that of HST. At this time, Cassini is high over Saturn's north pole at a local time of about 3 h. Hence, the bright feature on the right side of this image corresponds to the dawn brightening in the HST image in Fig. 7. The UVIS vantage point of just about 5.5 $R_S$ above the aurora provides significantly more detail. The pre-noon poleward feature also appears in the UVIS image.

## 3. Comparison of SKR and UV auroral power

In this section we compare the integrated power flux in SKR to the estimated input power to the UV aurora from HST images.

During the approach campaign in the first half of 2004, Kurth et al. (2005) looked for a correlation between the power input to the aurora, based on the intensity of the UV aurora and the integrated SKR power flux. While they did find a positive correlation, there were only two measurements of UV intensities that were significantly stronger than the others available, hence, the correlation was heavily based on those two measurements. The remaining ones were clustered at relatively low intensities and showed no clear correlation. Here, we attempt a similar correlation, using all of the HST images during the spring 2013 campaign which fall into the three intervals discussed above.

Fig. 9 superposes the time history of SKR integrated power flux with measurements of the power input to the aurora based on the

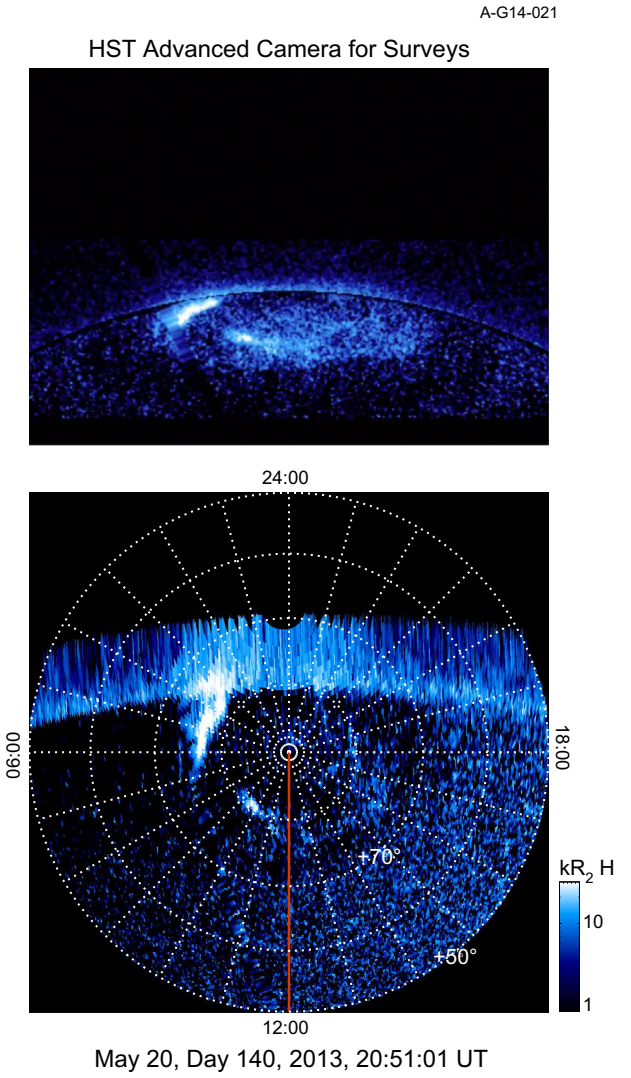


**Fig. 7.** HST images obtained at the time indicated by the arrow in Fig. 6.

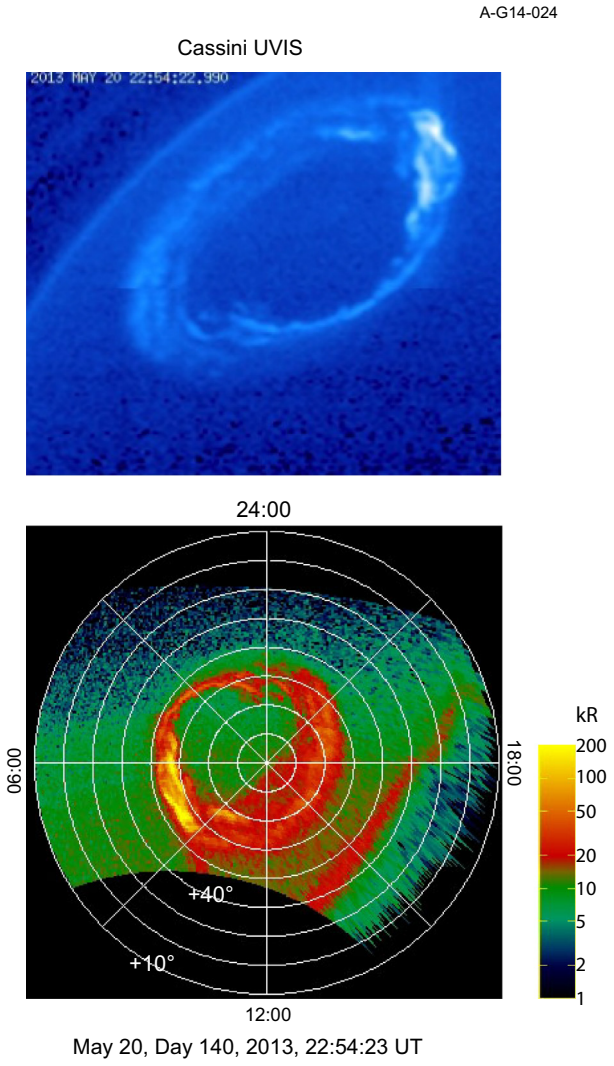


**Fig. 8.** UVIS image acquired at the time indicated by the arrow in Fig. 6. Note the point of view of this image is set by Cassini's position in orbit at Saturn, above the pre-dawn sector near 2.8 h local time.

UV intensities. The SKR observations are 10-h averages slid by 1 h and, again, are integrated from 20 kHz to 1 MHz, as was done in Fig. 1 above. The UV power $P_{UV}$, is the result of averaging over the 44 min of observations on each of the HST orbits used for the Saturn observations. The auroral intensity in kR is computed from observed counts using the (Gustin et al., 2012) conversion values for a color ratio of 1.1, and the total power is then computed by summing the emission over the auroral region, and assuming a mean $H_2$ photon energy of $1.6 \times 10^{-18}$ J. This gives the total power in the unabsorbed $H_2$ emission over the range 700–1800 Å, excluding the H Lyman lines (which contribute a further 10%). The power values given are the mean of that derived from the F125LP images in each orbit. The two scales used in Fig. 9 were selected so as to have similar dynamic ranges, but no attempt was made to fit the data in any statistical manner. Nevertheless, the values of $P_{UV}$ follow the trend in the SKR power flux quite well, providing some hope of a reasonable correlation.

In Fig. 10 we plot $P_{UV}$ vs $P_{SKR}$ in a log–log plot. These values use the 10-h averages for $P_{SKR}$ plotted in Fig. 9 for the time centered at the time of the determination of $P_{UV}$. We then do a linear fit to the data with the function

$$P_{UV} = 10^x P_{SKR}^y \quad (1)$$

The fit parameters for this are $x = 3.404 \pm 0.224$ and $y = 0.161 \pm 0.020$. Of course, the first factor is a constant = 2535. The coefficient of determination for the fit $R^2$ is 0.82, and $P < 0.0001$. Further, we note the more satisfactory spread in power across the dynamic range for this set of measurements than those used in the Kurth et al. (2005) analysis. This fit did not use the point represented by an 'x' in Fig. 10. This point came from a 10-h averaging interval on day 140 starting at 12:49 which included much of the periapsis interval in which the upper hybrid resonance frequency, hence, the cutoff of the R–X mode rose well into the SKR frequency range. This is also the radial distance range where the $r^{-2}$ correction is subject to large errors. By including this point, the $R^2$ parameter decreases to 0.59 although the fit parameters do not change appreciably; $x = 3.29$ and $y = 0.149$.

We chose 10 h as an interval over which to average the power flux in the SKR because previous studies (c.f., Kurth et al., 2005; Lamy et al., 2013) have shown that beaming of the SKR limits the visibility to a given observer at a given time. Averaging over a Saturn rotation is believed to reduce the effects of beaming, assuming the intensity of SKR emitted in all directions is constant. This assumption is not likely to be valid, but it seems to be a better assumption than that of assuming the observer is always in the

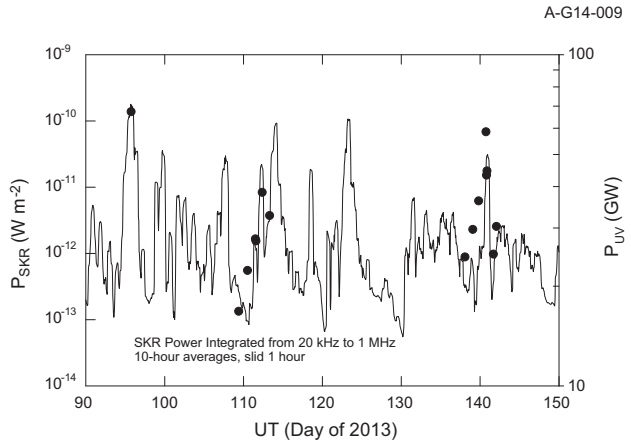


**Fig. 9.** Overlay of power input to Saturn's aurora based on UV intensities from HST imaging and integrated SKR power flux from 20 kHz to 1 MHz. No mathematical relation was used to set the UV and SKR power scales used in this figure; they were adjusted to illustrate the apparent relation between the two indicators of auroral activity.

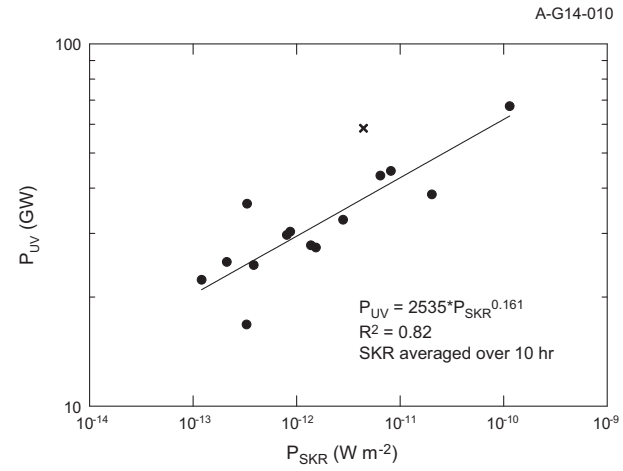


**Fig. 10.** A scatter plot of power input to the aurora determined from HST imaging and 10-h averages of SKR power integrated from 20 kHz to 1 MHz centered on the times for the images. The fit was over all points except for the '*x*' as explained in the text.

beaming pattern of the radio emissions. However, to investigate this further, we have repeated the experiment using 44-min averages of SKR that match the acquisition times for the UV images and the averaging interval for the UV power. The result is shown in Fig. 11. In fact, the fit parameters are very similar to those using the 10-h SKR averages with $x = 3.362 \pm 0.465$ and $y = 0.157 \pm 0.041$ (the first factor being 2301). However, the distribution of points along the fit is more scattered and the $R^2$ is only 0.55. The poorer correlation is consistent with the findings of Lamy et al. (2013) that it is important to average the SKR power of a time suitable for all of the radio sources to rotate though the RPWS radio beam. This result tends to increase our inclination to use an SKR averaging interval close to a rotation period, but also indicates that the longer average does not seem to affect the relationship between $P_{UV}$ and $P_{SKR}$, appreciably. It should also be noted that by combining the observations over the three intervals as done here, we have introduced another variable – that of measurements obtained in different locations. Since there are local time and latitudinal variations in the observed intensities of SKR (Lamy et al., 2008), these variations will decrease the correlation

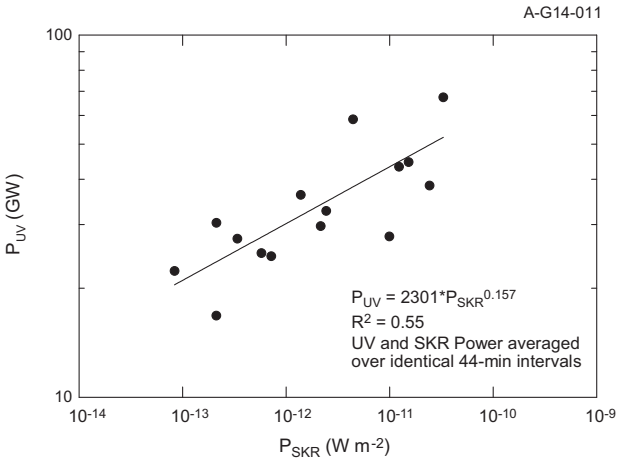


**Fig. 11.** A comparison of power input to the aurora based on HST UV images an SKR power integrated from 20 kHz to 1 MHz for the same 44-min intervals used for acquiring the images. While the fit is very similar to that shown in Fig. 10 for 10-h SKR averages, the coefficient of determination $R^2$ is smaller. This is likely a result of not averaging over a sufficient time for Cassini to be exposed to the SKR beams from all of the radio sources distributed through Saturn's polar regions.

between the observed SKR integrated power flux and the power in the UV aurora.

## 4. Summary and conclusions

This paper presents observations of Saturn kilometric radiation during the spring 2013 Saturn auroral campaign as a means of providing some measure of auroral activity over the campaign given that such a campaign cannot support anything close to continuous monitoring at UV, visual, or IR wavelengths. Given the known influence of solar wind dynamics on both SKR intensity (Desch, 1982) and auroral activity at Saturn (e.g. Crary et al., 2005; Clarke et al., 2005), the SKR integrated power is also a proxy for solar wind activity. This is because the RPWS antenna system provides nearly 4 steradians of visibility to SKR wavelengths, meaning spacecraft attitude does not preclude detection of the signal. (It is important to say that the antenna geometry IS important for the successful employment of radio direction-finding and polarization studies of the SKR.) We have shown that there is a good correlation between 10-h averages of SKR power flux and the power estimated input to the aurora on the basis of the UV brightness, justifying the SKR as a simple proxy for auroral activity through the campaign. Certainly, as pointed out by Lamy et al. (2013), the instantaneous SKR power flux is difficult to interpret given the highly anisotropic and beaming properties of the emission and the complex, distributed set of radio sources present at any given time in Saturn's polar regions.

The SKR emissions give evidence for a recurrent pattern of solar wind interaction with Saturn's magnetosphere, suggesting a two-sector structure and associated corotating interaction regions influencing the level of auroral activity on Saturn. But there are other SKR intensifications that may be due to internal processes.

## Acknowledgments

Re-projected HST images are from the Auroral Planetary Imaging and Spectroscopy (APIS) database (http://lesia.obspm.fr/apis) at LESIA/VO-Paris Data Centre (Observatoire de Paris, CNRS). The research at the University of Iowa was supported by NASA through Contract 1415150 with the Jet Propulsion Laboratory. The research in Meudon is supported by CNES. EJB is supported by the STFC Leicester Consolidated Grant ST/K001000/1, and a Philip Leverhulme Award.

## References


Badman, S.V., Cowley, S.W.H., et al., 2008. Relationship between solar wind corotating interaction regions and the phasing and intensity of Saturn kilometric radiation bursts. Ann. Geophys. 26 (12), 3641–3651.

Badman, S.V., et al., 2016. Saturn's auroral morphology and field-aligned currents during a solar wind compression. Icarus 263, 83–93.

Brown, R.H. et al., 2004. The Cassini visual and infrared mapping spectrometer (VIMS) investigation. Space Sci. Rev. 115, 111–168.

Bunce, E.J., Cowley, S.W.H., Milan, S.E., 2005a. Interplanetary magnetic field control of Saturn's polar cusp aurora. Ann. Geophys. 23, 1405–1431.

Bunce, E.J. et al., 2005b. In situ observations of a solar wind compression-induced hot plasma injection in Saturn's tail. Geophys. Res. Lett. 32, L20S04. http://dx.doi.org/10.1029/2005GL022888.

Burlaga, L.F. et al., 2003. Evolution of magnetic fields in corotating interaction regions from 1 to 95 AU: Order to chaos. Astrophys. J. 590, 554–566.

Clarke, J.T. et al., 2005. Morphological differences between Saturn's ultraviolet aurorae and those of Earth and Jupiter. Nature 433, 717–719.

Clarke, J.T. et al., 2009. The response of Jupiter's and Saturn's auroral activity to the solar wind. J. Geophys. Res. 114, A05210. http://dx.doi.org/10.1029/2008JA013694.

Crary, F.J. et al., 2005. Solar wind dynamic pressure and electric field as the main factors controlling Saturn's aurorae. Nature 433, 720–722.

Desch, M.D., 1982. Evidence for solar wind control of Saturn radio emission. J. Geophys. Res. 87, 4549–4554.

Desch, M.D., 1983. Radio emission signature of Saturn immersions in Jupiter's magnetic tail. J. Geophys. Res. 88, 6904–6910.

Desch, M.D., Kaiser, M.L., 1981. Voyager measurements of the rotation period of Saturn's magnetic field. Geophys. Res. Lett. 8, 253–256.

Dougherty, M.K. et al., 2004. The Cassini magnetic field investigation. Space Sci. Rev. 114, 331–383.

Esposito, L.W. et al., 2004. The Cassini ultraviolet imaging spectrograph investigation. Space Sci. Rev. 115, 299–361.

Gérard, J.-C. et al., 2005. Signature of Saturn's auroral cusp: Simultaneous Hubble Space Telescope FUV observations and upstream solar wind monitoring. J. Geophys. Res. 110, A11201. http://dx.doi.org/10.1029/2005JA011094.

Grodent, D. et al., 2005. The global morphology of Saturn's southern ultraviolet aurora. J. Geophys. Res. 110, A01207. http://dx.doi.org/10.1029/2004JA010717.

Gurnett, D.A., 1974. The Earth as a radio source: terrestrial kilometric radiation. J. Geophys. Res. 79, 4227–4238.

Gurnett, D.A. et al., 2002. Control of Jupiter's radio emission and aurorae by the solar wind. Nature 415, 985–987.

Gurnett, D.A. et al., 2004. The Cassini radio and plasma wave science investigation. Space Sci. Rev. 114, 395–463.

Gurnett, D.A. et al., 2009. Discovery of a north-south asymmetry in Saturn's radio rotation period. Geophys. Res. Lett. 36, L16102. http://dx.doi.org/10.1029/2009GL039621.

Gustin, J. et al., 2012. Conversion from HST ACS and STIS auroral counts into brightness, precipitated power, and radiated power for H2 giant planets. J. Geophys. Res. 117, A07316. http://dx.doi.org/10.1029/2012JA017607.

Hess, S.L.G. et al., 2014. Multi-instrument study of the jovian radio emissions triggered by solar wind shocks and inferred magnetospheric subcorotation rates. Planet. Space Sci. 99, 136–148.

Hsu, H.-W., et al., 2016. Solar wind magnetic field structure at Saturn during the 2013 aurora campaign, Icarus 263, 10–16.

Huff, R.L. et al., 1988. Mapping of auroral kilometric radiation sources to the aurora. J. Geophys. Res. 93, 11,445–11,454.

Jackman, C.M. et al., 2005. Interplanetary conditions and magnetospheric dynamics during the Cassini orbit insertion fly-through of Saturn's magnetosphere. J. Geophys. Res. 110, A10212. http://dx.doi.org/10.1029/2005JA011054.

Jackman, C.M. et al., 2009. On the character and distribution of lower-frequency radio emissions at Saturn, and their relationship to substorm-like events. J. Geophys. Res. 114, A08211. http://dx.doi.org/10.1029/2008JA013997.

Krimigis, S.M. et al., 2004. Magnetosphere imaging instrument (MIMI) on the Cassini mission to Saturn/Titan. Space Sci. Rev. 114, 233–329.

Kurth, W.S., Gurnett, D.A., 1998. Auroral kilometric radiation integrated power flux as a proxy for AE. Adv. Space Res. 22 (1), 73–77.

Kurth, W.S. et al., 1998. Auroral kilometric radiation and the Auroral Electrojet Index for the January 1997 magnetic cloud event. Geophys. Res. Lett. 25, 3027–3030.

Kurth, W.S. et al., 2005. An Earth-like correspondence between Saturn's auroral features and radio emission. Nature 433, 722–725.

Kurth, W.S. et al., 2008. An update to a Saturn longitude system based on kilometric radio emissions. J. Geophys. Res. 113, A05222. http://dx.doi.org/10.1029/2007JA012861.

Lamy, L. et al., 2008. Saturn kilometric radiation: Average and statistical properties. J. Geophys. Res. 113, A07201. http://dx.doi.org/10.1029/2007JA012900.

Lamy, L. et al., 2009. An auroral oval at the footprint of Saturn's kilometric radio sources, colocated with the UV aurorae. J. Geophys. Res. 114, A10212. http://dx.doi.org/10.1029/2009JA014401.

Lamy, L., 2011. Variability of southern and northern periodicities of Saturn kilometric radiation. In: Rucker, H.O., Kurth, W.S., Louarn, P., Fischer, G., (Eds.), Planetary Radio Emissions VII, Austrian Academy of Sciences, Vienna, Austria, pp. 38–50.

Lamy, L. et al., 2013. Multispectral simultaneous diagnosis of Saturn's aurorae throughout a planetary rotation. J. Geophys. Res. 118, 4817–4843. http://dx.doi.org/10.1002/jgra.50404.

Lecacheux, A., Galopeau, P., Aubier, M., 1997. Re-visiting Saturnian radiation with Ulysses/URAP. In: Rucker, H.O., Bauer, S.J., Lecacheux, A. (Eds.), Planetary Radio Emissions IV. Austrian Academy of Sciences Press, Vienna, pp. 313–325.

Louarn, P. et al., 2000. A Study of the jovian energetic magnetospheric events observed by Galileo: Role in the radial plasma transport. J. Geophys. Res. 105, 13,073–13,088.

Louarn, P. et al., 2001. A multi-instrument study of a jovian magnetospheric disturbance. J. Geophys. Res. 106, 29,883–29,898.

Louarn, P. et al., 2007. Observation of similar radio signatures at Saturn and Jupiter: Implications for the magnetospheric dynamics. Geophys. Res. Lett. 34, L20113. http://dx.doi.org/10.1029/2007GL030368.

Louarn, P., Paranicas, C.P., Kurth, W.S., 2014. Global magnetodisk disturbances and energetic particle injections at Jupiter. J. Geophys. Res. 119, 4495–4511.

Murata, T. et al., 1997. Correlations of AKR index with Kp and Dst indices. Proc. NIPR Syrup. Upper Atmos. Phys. 10, 64–68.

Nichols, J.D. et al., 2009. Saturn's equinoctial auroras. Geophys. Res. Lett. 36, L24102. http://dx.doi.org/10.1029/2009GL041491.

Nichols, J.D. et al., 2014. Dynamic auroral storms on Saturn as observed by the Hubble Space Telescope. Geophys. Res. Lett. 41. http://dx.doi.org/10.1002/2014GL060186.

Porco, C.C. et al., 2004. Cassini imaging science: Instrument characteristics and anticipated scientific investigations at Saturn. Space Sci. Rev. 115, 363–497.

Prangé, R. et al., 2004. A CME-driven interplanetary shock traced from the Sun to Saturn by planetary auroral storms. Nature 432, 78–81. http://dx.doi.org/10.1038/nature02986.

Voots, G.R., Gurnett, D.A., Akasofu, S.-I., 1977. Auroral kilometric radiation as an indicator of auroral magnetic disturbances. J. Geophys. Res. 82, 2259–2266.

Wang, Z. et al., 2010. Cassini observations of narrowband radio emissions in Saturn's magnetosphere. J. Geophys. Res. 115, A06213. http://dx.doi.org/10.1029/2009JA014847.

Ye, S.-Y. et al., 2009. Source locations of narrowband radio emissions detected at Saturn. J. Geophys. Res. 114, A06219. http://dx.doi.org/10.1029/2008JA013855.

Ye, S.-Y. et al., 2010. Z-mode waves as the source of Saturn narrowband radio emissions. J. Geophys. Res. 115, A08228. http://dx.doi.org/10.1029/2009JA014167.

Zieger, B., Hansen, K.C., 2008. Statistical validation of a solar wind propagation model from 1 to 10 AU. J. Geophys. Res. 113, A08107. http://dx.doi.org/10.1029/2008JA01304.